Role of Water Molecules in Enhancing the Proton Conductivity on Reduced Graphene Oxide under High Humidity

Gum-Chol Ri, Jin-Song Kim, and Chol-Jun Yu*

Department of Computational Materials Design, Faculty of Materials Science, Kim Il Sung University, Ryongnam-Dong, Taesong District, Pyongyang, Democratic People's Republic of Korea

(Received 17 January 2018; revised manuscript received 25 May 2018; published 11 September 2018)

Recent experimental reports on in-plane proton conduction in reduced graphene oxide (rGO) films open a new way for the design of a proton-exchange membrane essential for fuel cells and chemical filters. In humid conditions, water molecules attached to the rGO sheet are expected to play a critical role in this membrane, but theoretical studies of their involvement are scarcely found in the literature. In this study, we investigate proton migration on water-adsorbed monolayer and bilayer rGO sheets using first-principles calculations to reveal the mechanism. We devise a series of models for water-adsorbed rGO films by systematically varying the reduction degree and water content, and we optimize their atomic structures in reasonable agreement with experiments using a density functional that accounts for van der Waals correction. After suggesting two different transport mechanisms, epoxy-mediated hopping and water-mediated hopping, we determine the kinetic activation barriers for these in-plane proton transports on the rGO sheets. Our calculations indicate that water-mediated transport is more likely to occur due to its much lower activation energy than epoxy-mediated transport and reveal new prospects for developing efficient solid proton conductors.

DOI: 10.1103/PhysRevApplied.10.034018

I. INTRODUCTION

A proton-exchange membrane is an essential component in electrochemical-energy-generating and electrochemical-energy-storage devices such as fuel cells and batteries as well as selective material sieving systems such as sensors and chemical filters. Nafion and Nafion-based artificial materials have been widely used as an efficient proton-exchange membrane, but they have serious problems, such as high cost and conductivity loss at temperatures above 353 K [1–3]. Recently, graphene oxide (GO) and reduced GO (rGO) films with a controlled reduction degree have attracted considerable attention as a superior solid electrolyte for proton exchange to Nafion due to their low cost, easy fabrication, and environmental friendliness [4–7].

Protons can pass across monolayer graphene [8–10] or a few-layer GO sheet [4–6], and even water molecules can pass across a rGO sheet [11], but only through atomic-scale defects created on those nanosheets. If there is no defect, graphene and GO sheets are impermeable to protons under ambient conditions due to a dense, delocalized-electron cloud formed by the π orbitals of graphene [12,13]. Hu *et al.* [8] measured the proton areal conductivity across a monolayer graphene sheet as $\sigma = S/A \approx$ 2–4 mS/cm^2 ($S = I/V$ is the conductance and A is the area of the sample) at room temperature, with a corresponding activation barrier of $E_a \approx 0.78$ eV. For such proton transport, first-principles calculations yielded even higher values of 1.25–1.56 eV due to different proton-transport pathways from experiments such as transport in a vacuum rather than in an aqueous environment [14–17]. Decorating graphene with catalytic metal nanoparticles such as Pt nanoparticles reduces the activation barrier by approximately 0.5 eV [8], which is still relatively high. Therefore, research has focused on creating nanopores with a precisely controlled narrow size distribution on multilayer graphene or GO films to achieve easy passage of protons [18]. In these porous multilayer films, protons can move in one layer and pass to another through nanopores [19]. Then the problem changes from the through-plane conductivity to the in-plane conductivity, but the activation barrier for proton or hydrogen-atom transport on a graphene sheet is still high, 0.9 eV, due to a strong binding of hydrogen to the graphene sheet [20].

Unlike graphene, GO has oxygenated functional groups such as epoxy (—O—) and hydroxy (—OH) groups, which form one-dimensional hydrogen-bonded channels for proton transport [21–25]. Hatakeyama *et al.* [26–31] reported that multilayer GO films have high in-plane proton conductivity at room temperature and high relative humidity (RH). They measured the in-plane proton conductivity of rGO film to be $\sigma = (S \times L)/(T \times D) \approx 2.4$ mS/cm (L, T, and D are the width, thickness, and length of the sample) at 278 K and 90% RH, with a corresponding activation

*ryongnam14@yahoo.com

barrier of 0.12 eV. When some functional groups were added to GO, forming, for example, GO-Nafion hybrid [3,32] or sulfonated GO complexes [26,28,30,33], the in-plane proton conductivity was enhanced. These experimental findings imply that uptake and retention of water in the GO sheet are a key factor for high proton conductivity; even for the case of graphene the activation barrier reduces by 0.42 eV when mediation is by water molecules [20]. It was expected that hydrophilic functional groups such as epoxy groups in the GO sheet can readily adsorb water molecules and support the channel formation for proton transport on the sheet. In this context, it is urgent to theoretically reveal the mechanism behind enhanced proton transport by water adhesion to a GO sheet for the design of a functional GO-based solid electrolyte. To the best of our knowledge, however, theoretical studies of these phenomena have been scarcely reported, although there are first-principles studies for proton penetration through graphene and other two-dimensional materials [8,14–17].

In this work, we investigate the atomic structures of water-adsorbed monolayer and bilayer rGO sheets and proton migration on these sheets by using a first-principles method within the density-functional-theory (DFT) framework. The van der Waals (vdW) dispersive interactions between the graphene sheets and molecules are included with use of the advantage of the vdW density functional OB86 method [34]. We predict the migration paths of protons on rGO sheets by estimating the bond valence sum (BVS) [35], and calculate the activation barriers for these in-plane proton migrations by using the climbing-image nudged-elastic-band (NEB) method [36]. On the basis of the calculation data, we propose the most reasonable mechanism for the enhancement of proton conductivity by water molecules.

II. COMPUTATIONAL METHODS

We first perform atomistic modeling of rGO sheets and build the corresponding supercells. For the types of rGO with different oxidation or reduction degrees, we consider both monolayer and bilayer rGO sheets with gradually increasing $O/(C+O)$ ratios from the minimum value of 14.3% to the maximum value of 33.3%. Orthogonal (6×3) and (4×2) cells are used for the basal plane of the graphene sheet, and contain 72 and 32 carbon atoms, respectively. On both sides of the graphene sheet, the same number of oxygen atoms are adsorbed to form epoxy groups. We arrange the epoxy groups as a continuous row to form a migration path for the in-plane proton transport, on the basis that the epoxy groups are clustered on the rGO sheet [21]. Then the number of oxygen atoms is 12 for the case of a (6×3) cell and 8, 12, or 16 for the case of a (4×2) cell, which correspond to the chemical formulas $C_{72}O_{12}$ [$O/(C+O) = 14.3\%$], $C_{32}O_8$ [$O/(C+O) = 20.0\%$], $C_{32}O_{12}$ [$O/(C+O) = 27.3\%$], and $C_{32}O_{16}$ [$O/(C+O) = 33.3\%$]. A simulated lattice constant of 2.46 Å and a vacuum layer of 15-Å thickness are used throughout the work.

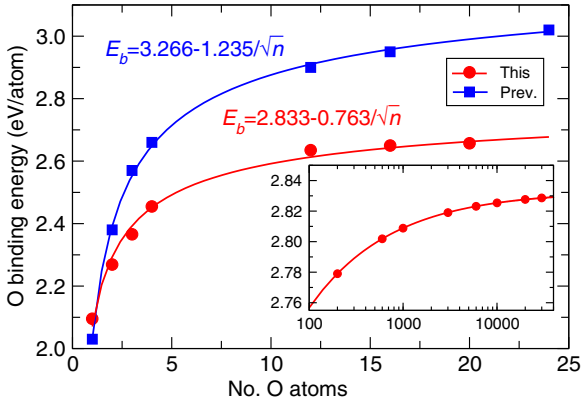

FIG. 1. Oxygen binding energy with increasing number of oxygen atoms in rGO. The inset shows an extension to more than 100 oxygen atoms using the interpolation curve. The blue line shows the previous theoretical result [21].

All calculations are performed with the pseudopotential plane-wave method as implemented in QUANTUM ESPRESSO (version 5.3) [37]. We use the Vanderbilt-type ultrasoft pseudopotentials to describe the interaction between ions and valence electrons [38]. The Perdew-Burke-Ernzerhof functional [39] within the generalized-gradient approximation is used for the exchange-correlation interaction between valence electrons. For the vdW dispersive interaction between the graphene sheets and water molecules, the vdW energy provided by the vdW density functional OB86 method [34] is added to the DFT total energy. As the major computational parameters, the plane-wave cutoff energies are set to be 40 Ry for the wave function and 400 Ry for the electron density, and the Monkhorst-Pack special k-points are set to be $(2 \times 2 \times 5)$ for a bilayer sheet and $(2 \times 2 \times 1)$ for a monolayer sheet, providing a total energy accuracy of 5 meV per carbon atom. The self-consistent convergence threshold for total energy is 10^{-9} Ry, and the convergence threshold for atomic force in structural relaxations is 8×10^{-4} Ry/bohr. The Methfessel-Paxton first-order smearing approach with a 0.2-eV Gaussian spreading factor is applied for structural optimizations and proton-transfer simulations, while the tetrahedron approach is applied for calculations of the electronic density of states.

We calculate the oxygen binding energy as a function of the number of oxygen atoms in rGO and compare it with previous data from first-principles calculations [21] to check the validity of the computational parameters and our rGO supercell models. The oxygen binding energy per atom E_b can be calculated as follows:

$$E_b = -\frac{1}{N_O}(E_{rGO} - E_G - N_O E_O), \tag{1}$$

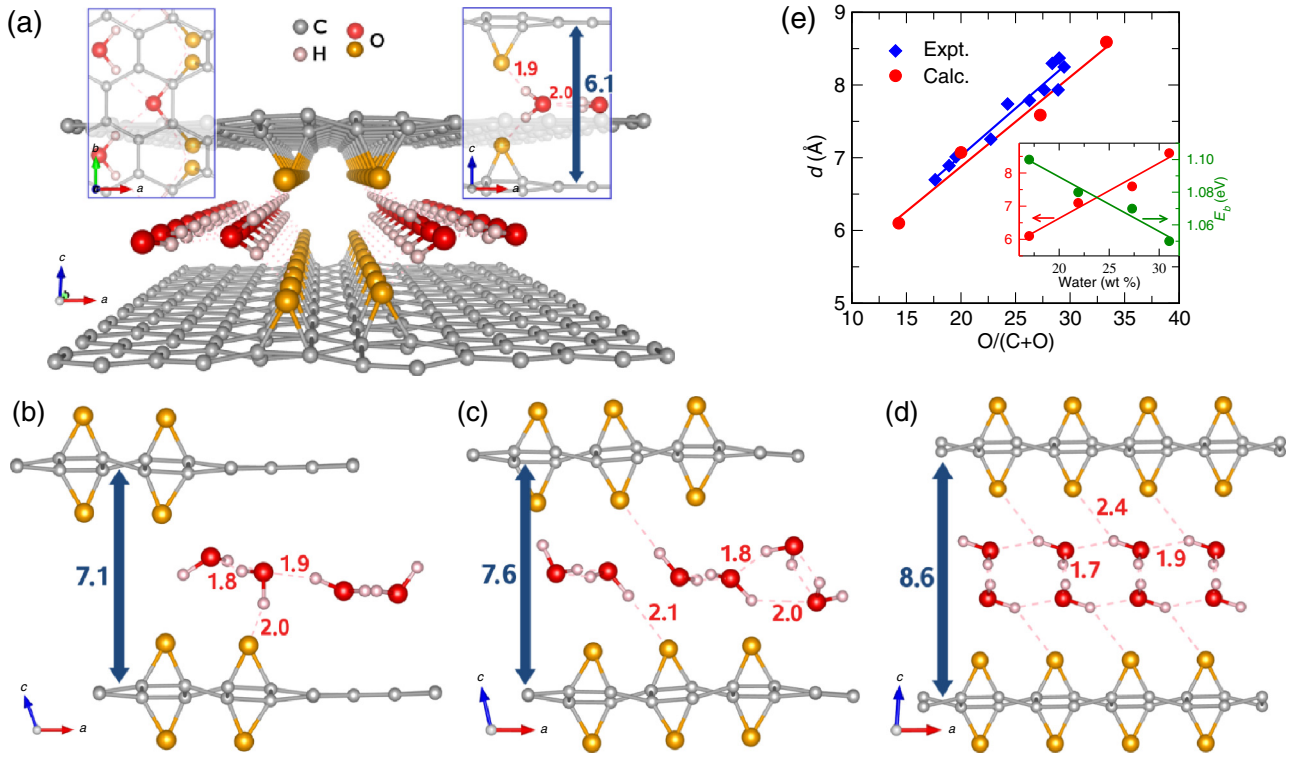

FIG. 2. Optimized atomic structures of water-intercalated bilayer rGO with chemical formula (a) $C_{72}O_{12} \cdot 12H_2O$ in perspective (center), top (left), and side (right) views and (b) $C_{32}O_8 \cdot 8H_2O$, (c) $C_{32}O_{12} \cdot 12H_2O$, and (d) $C_{32}O_{16} \cdot 16\ H_2O$ in side view. The interlayer distance and hydrogen-bond lengths in angstroms are shown. (e) Interlayer distance d as a function of oxidation degree [O/(C + O) (%)], where the experimental values are from Ref. [27] and the calculated values are from this work. The inset shows the interlayer distance and water binding energy per molecule (E_b) as a function of water content.

where E_{rGO}, E_G, and E_{O} are the total energies of rGO, graphene, and an isolated oxygen atom, and N_{O} is the number of oxygen atoms involved in the rGO model. The result is shown in Fig. 1. Similarly, the water binding energy per molecule can be calculated as follows:

$$E_b = -\frac{1}{N_{\mathrm{H_2O}}}(E_{\text{hyd-rGO}} - E_{\mathrm{rGO}} - N_{\mathrm{H_2O}}E_{\mathrm{H_2O}}), \qquad (2)$$

where $E_{\text{hyd-rGO}}$ and $E_{\mathrm{H_2O}}$ are the total energies of a water-adsorbed rGO supercell and an H_2O molecule, and $N_{\mathrm{H_2O}}$ is the number of water molecules. The proton adsorption energy in the water-adsorbed rGO sheet can be calculated as follows:

$$E_{\mathrm{ad}} = E_{\text{p-hyd-rGO}} - E_{\text{hyd-rGO}} - \frac{1}{2}E_{\mathrm{H_2}}, \qquad (3)$$

where $E_{\text{p-hyd-rGO}}$ and $E_{\mathrm{H_2}}$ are the total energies of proton-adsorbed hydrous rGO and an H_2 molecule.

To predict possible positions of protons inserted into the water-adsorbed rGO sheets, we apply the BVS method [35]. The BVS at position $\mathbf{r}$, $B(\mathbf{r})$, can be calculated as follows:

$$B(\mathbf{r}) = \sum_i \exp\left(\frac{R_0 - R_i(\mathbf{r})}{b}\right), \qquad (4)$$

where $R_i(\mathbf{r}) = |\mathbf{r} - \mathbf{R}_i|$ ($\mathbf{R}_i$ for oxygen positions), b (0.37 Å) is a constant, and R_0 is a constant specific to the pair of hydrogen and oxygen atoms. The constant R_0 is estimated with use of the atomic size (r) and electronegativity (c) as follows [40]:

$$R_0 = r_{\mathrm{H}} + r_{\mathrm{O}} - \frac{r_{\mathrm{H}}r_{\mathrm{O}}\left(\sqrt{c_{\mathrm{H}}} - \sqrt{c_{\mathrm{O}}}\right)^2}{c_{\mathrm{H}}r_{\mathrm{H}} + c_{\mathrm{O}}r_{\mathrm{O}}}, \qquad (5)$$

where $r_{\mathrm{H}} = 0.38$ Å, $r_{\mathrm{O}} = 0.63$ Å, $c_{\mathrm{H}} = 0.89$, and $c_{\mathrm{O}} = 3.15$ [41]. The values of $B(\mathbf{r})$ at the positions of the hydrogen atoms are evaluated to be almost 3, and the difference of $B(\mathbf{r})$ from this value is calculated for the whole space with a grid resolution of 0.1 Å.

To calculate the migration barriers for the in-plane proton transport, we use the NEB method [36]. The supercell dimensions are fixed at the optimized supercell size during the NEB runs, while all the atoms are relaxed until the forces converge to within 0.05 eV/Å. The number of images is tuned so that the distance between neighboring NEB images is less than 1 Å. Both the image

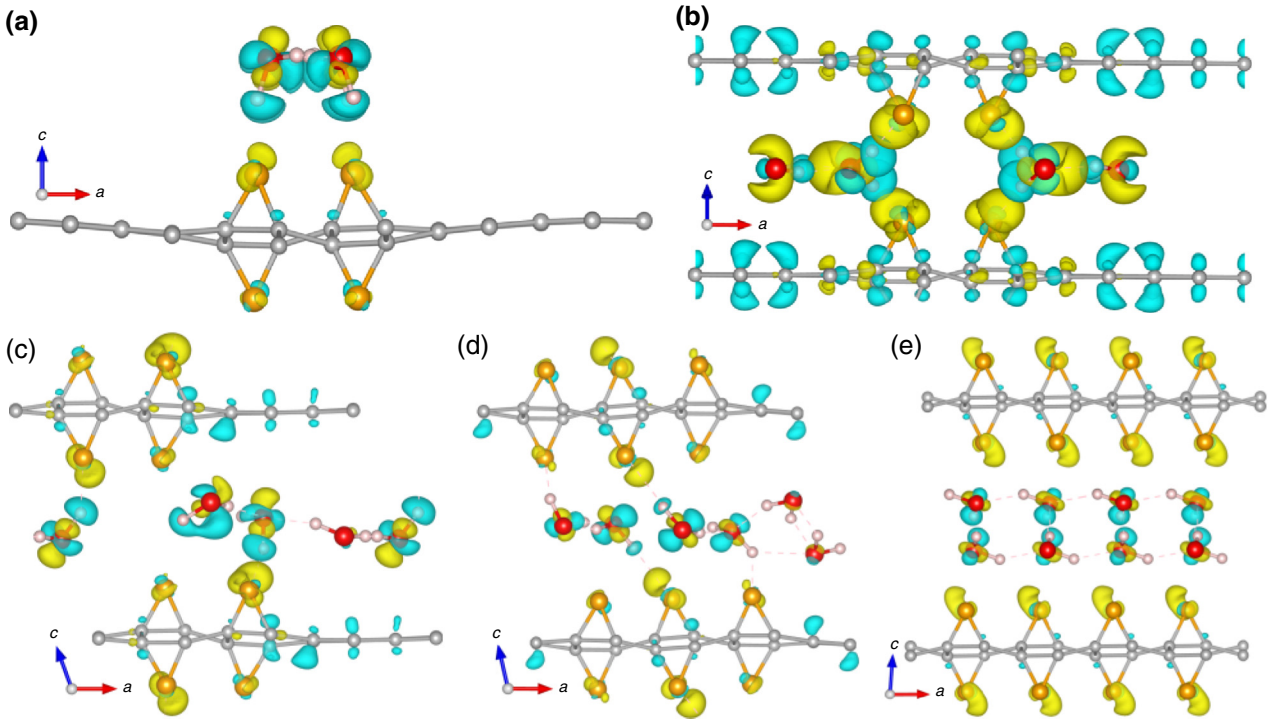

FIG. 3. Isosurface plot of electronic charge density difference between hydrous and anhydrous states of (a) monolayer $C_{72}O_{12} \cdot 6H_2O$, (b) bilayer $C_{72}O_{12} \cdot 12H_2O$, (c) bilayer $C_{32}O_8 \cdot 8H_2O$, (d) bilayer $C_{32}O_{12} \cdot 12H_2O$, and (e) bilayer $C_{32}O_{16} \cdot 16H_2O$ rGO at a value of 0.002 $|e|/Å^3$. Yellow (cyan) represents the charge accumulation (depletion). Small gray and pink balls represent carbon and hydrogen atoms, while brown and red balls represent oxygen atoms of the epoxy group and water molecule, respectively.

energies and their derivatives are used to interpolate the path energy profile that passes exactly through each image, as implemented in the neb.x code included in QUANTUM ESPRESSO [37].

III. RESULTS AND DISCUSSION

A. Atomic structures

We check the validity of the computational parameters and supercell models by estimating the oxygen binding energy per atom in monolayer rGO sheets with (6×3) cells by increasing the number of oxygen atoms ($n = 1$, 2, 3, 4, 12, 16, 20). For the cases of $n = 12$, 16, and 20, the epoxy groups are arranged to form a row as mentioned earlier. We perform the atomic relaxations of these monolayer rGO supercells and calculate the oxygen binding energies, confirming that they agree well with previous results [21], as shown in Fig. 1. In the special case of $C_{72}O_{12}$, the value of 2.64 eV in this work is in reasonable agreement with the previous value of 2.90 eV. Furthermore, interpolation of the calculation data into a square-root function of the oxygen number gives the function $E_b(n) = 2.83 - 0.76/\sqrt{n}$ (eV), which is comparable with the previous result, $E_b(n) = 3.27 - 1.24/\sqrt{n}$ (eV). We emphasize that although our calculation data are slightly underestimated compared with the previous data, possibly due to a difference in the computational method from the previous work, the increasing tendencies are coincident with each other as the square-root function of the oxygen number.

Water molecules are allowed to be adsorbed on the monolayer rGO sheet or intercalated into the interlayer space in the bilayer rGO sheets. The intercalated water molecules are placed at the center of the carbon hexagon of the graphene sheet in the bilayer rGO, while the adsorbed water molecules are anchored to the epoxy groups on the monolayer rGO sheet, weakly binding with the epoxy oxygen atoms through hydrogen-bonding interaction. We consider a series of rGO films with gradually increasing water content by controlling the number of water molecules, such as monolayer $C_{72}O_{12} \cdot 6H_2O$ (water content 9.3 wt%) and bilayer $C_{72}O_{12} \cdot 12H_2O$ (water content 17.0 wt%), $C_{32}O_8 \cdot 8H_2O$ (water content 21.9 wt%), $C_{32}O_{12} \cdot 12H_2O$ (water content 27.3 wt%), and $C_{32}O_{16} \cdot 16H_2O$ (water content 31.0 wt%). Water contents of 21 and 31 wt% correspond to about 30% and 90% RH, respectively, in previous experimental work [19,42,43], indicating that low-, intermediate-, and high-humidity conditions are considered in this work.

We perform variable cell relaxations of these water-intercalated rGO supercells allowing atoms to be relaxed but only atomic relaxations for the monolayer rGO supercells. The optimized atomic structures of the

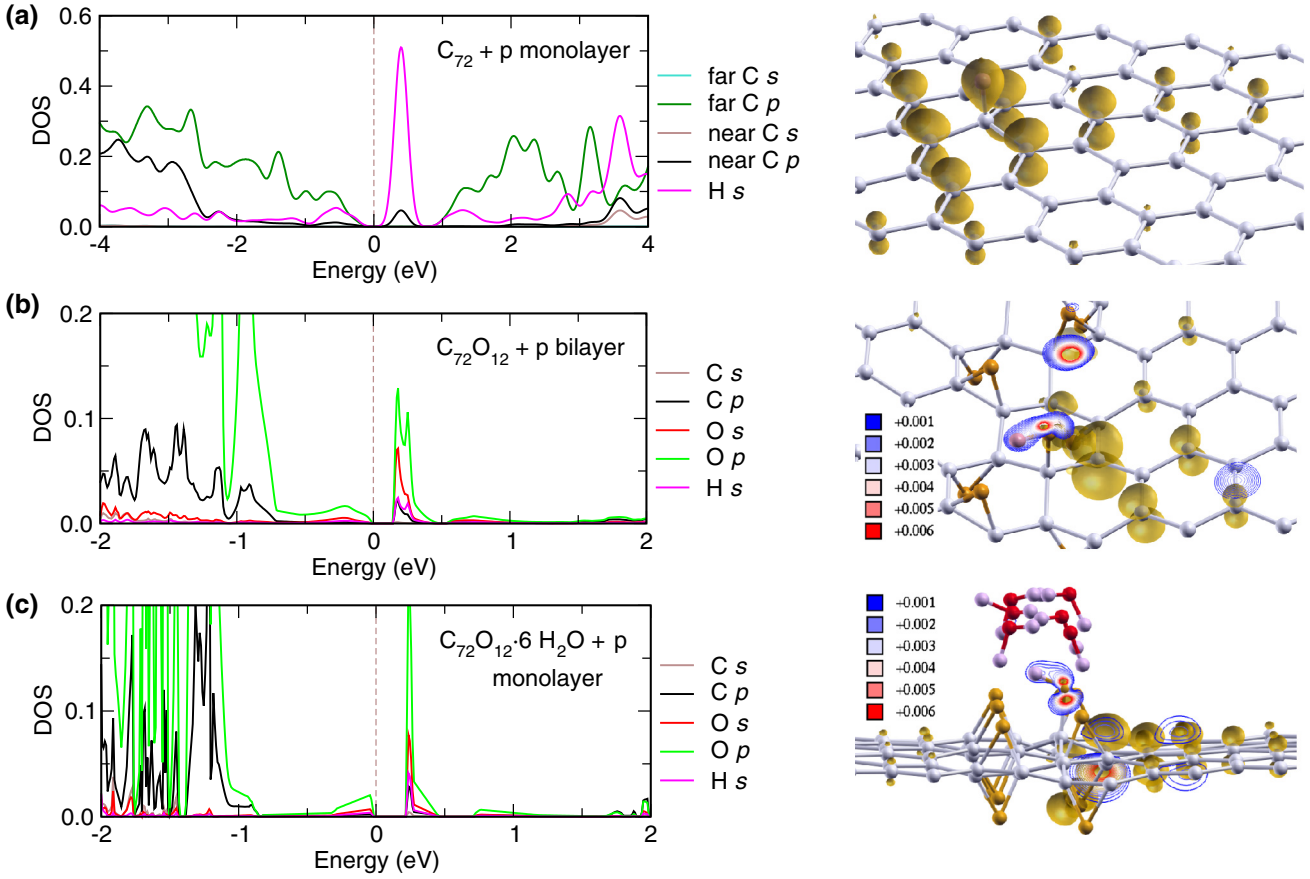

FIG. 4. Electronic density of states (DOS; left panel) and integrated local density of states (ILDOS; right panel) in charged supercells for (a) monolayer C_{72} with one proton, (b) bilayer $C_{72}O_{12}$ with one proton, and (c) monolayer $C_{72}O_{12} \cdot 6H_2O$ with one proton. The Fermi energy (E_F) is set to be zero in the DOS plot and the ILDOS is drawn in the energy range from 0 to 0.5 eV.

water-intercalated bilayer rGO sheets are shown in Figs. 2(a)–2(d), where their interlayer distances and hydrogen-bond lengths are also indicated. For the bilayer models the interlayer distance increases from 6.1 to 8.6 Å as a linear function of the oxidation degree, agreeing well with distances in rGO films prepared by a photoreduction process [27], as shown in Fig. 2(e). On the other hand, we see in the inset in Fig. 2(e) that the interlayer distance increases but the water binding energy decreases from 1.10 to 1.05 eV, both as linear functions of water content. The increase of interlayer distance with increasing water content is obvious given that the epoxy oxygen atoms attract water molecules through hydrogen-bonding interaction and thus more oxygen atoms can bind more water molecules, resulting in expansion of the interlayer space. In the case of the monolayer $C_{72}O_{12} \cdot 6H_2O$ model, the water binding energy is calculated to be 0.96 eV, being lower than in the bilayer models.

Hydrogen bonds are observed between the water molecule themselves, which are of zigzag type on the plane parallel to the basal graphene sheet, as shown in Fig. 2(a), and between the epoxy oxygen atoms and water molecules. While the the lengths of the hydrogen bonds between the water molecules are more or less invariable with a mean value of 1.9 Å, the lengths of the hydrogen bonds involving epoxy oxygen atoms increase gradually from 1.9 Å at a water content of 17.0% to 2.0, 2.1, and 2.4 Å at water contents of 21.9%, 27.3%, and 31.0%, respectively. This gradual increasing tendency of the length of the hydrogen bond between the epoxy oxygen atom and a water molecule with increasing water content is consistent with that of the water binding energy, indicating a weakening of hydrogen-bonding interaction in high-humidity conditions. The lengths in the monolayer $C_{72}O_{12} \cdot 6H_2O$ sheet are 1.7 Å for the former hydrogen bonds and 2.3 Å for the latter hydrogen bonds.

Figure 3 shows the electronic-charge-density difference when the water-adsorbed or water-intercalated rGO sheets are formed. It is clear that electronic charge transfer occurs on the uptake of water into rGO sheets, where carbon and hydrogen atoms donate electrons and oxygen atoms receive them. This charge transfer becomes weaker with increasing water content. The benefit of GO or rGO compared with pristine graphene is that it is easy to hold water

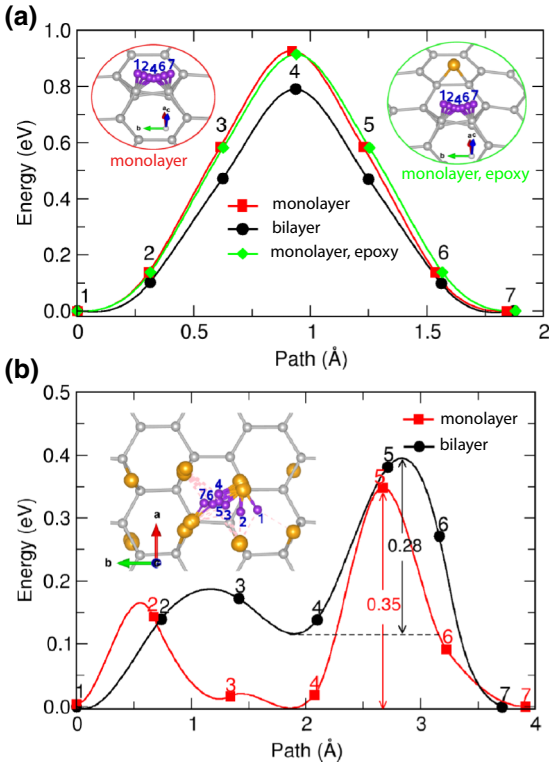

FIG. 5. Activation energy for proton migration (a) along the C—C bond in monolayer graphene (red), bilayer graphene (black), and monolayer graphene with one epoxy group (green) and (b) along the one-dimensional hydrogen-bonded channel formed by epoxy and hydroxy groups in monolayer GO (red) and bilayer GO (black) with the $C_{72}O_{12}$ model. The insets show the corresponding migration paths, where small balls denoted with numbers in purple indicate proton positions.

molecules through hydrogen-bonding interaction due to their functional groups, such as epoxy and/or hydroxy groups.

B. In-plane proton transport

Using the determined structures from the models, we proceed to study in-plane proton transport on rGO sheets. For the proton simulations, we insert a hydrogen atom into the appropriate position of the optimized or relaxed supercells as discussed earlier, and allow the supercells to be charged with one electron missing from the system. To make it clear whether the electron will be removed from the hydrogen atom, we present the electronic density of states and the integrated local density of states in typical systems such as monolayer C_{72}, bilayer $C_{72}O_{12}$, and monolayer $C_{72}O_{12} \cdot 6H_2O$ in Fig. 4. In these plots, only the density of states of the inserted H atom and the nearest C and O atoms and the integrated local density of states in the energy range from 0 to 0.5 eV when the Fermi energy is set to be zero are shown for clarity. In these three systems, we observe the empty *s*-type state of the hydrogen atom above the Fermi level, indicating its transition to a proton. When hydrogen forms a certain chemical bond with another element in a compound, it delivers an electron to become a proton, and thus it is not meaningful to distinguish the inserted hydrogen atom from the one bonded with the oxygen atom of a water molecule in the hydrous-rGO systems. In this context, the empty state of C and O atoms observed above the Fermi level can be explained by chemical bonding.

As a preliminary check for the difficulty of in-plane proton transport on a graphene sheet, we first consider proton migration on monolayer and bilayer graphene sheets. In these cases the proton can be adsorbed on top of the carbon atom with adsorption energies of −3.10 eV (monolayer) and −13.87 eV (bilayer), and migrates along the C—C bond with an activation energy of 0.93 eV in the monolayer, which is in good agreement with the previous result [20], and 0.79 eV in the bilayer, as can be seen in Fig. 5(a). The existence of an epoxy group around the migration path slightly reduces the activation energy by 0.91 eV, possibly due to the hydrogen-bonding interaction between the proton and the oxygen atom. At this point, it is worth noting that the oxygen atoms or epoxy groups should form a row rather than a randomized distribution on graphene, making a kind of "epoxy bridge" for fast in-plane proton migration; otherwise the proton should pass along the C—C bond, which has a higher activation barrier.

We next consider proton transport on a rGO sheet using the $C_{72}O_{12}$ model, where the proton is adsorbed on top of the epoxy oxygen atom to form a hydroxy group [44] with adsorption energies of −7.37 and −14.47 eV for the monolayer and bilayer sheets. The proton of the hydroxy group is enforced to hop to the neighboring epoxy oxygen atom (i.e., —OH → —O—) with activation energy of 0.35 eV for the monolayer rGO sheets and 0.28 eV for the bilayer rGO sheets, as shown in Fig. 5(b). This confirms that the one-dimensional hydrogen-bonded channels formed by epoxy groups on the rGO sheet can remarkably reduce the activation energy for in-plane proton transport [22–25]. In both cases of graphene and rGO sheets, bilayer sheets have lower activation energy than monolayer sheets, indicating that enhanced hydrogen-bonding interaction makes the proton transport fast.

For the cases of water-adsorbed or water-intercalated rGO sheets, it is not easy to clarify the adsorption sites and migration paths of protons. We propose two different transport mechanisms—namely, epoxy-mediated hopping and water-mediated proton hopping—in which protons of the hydroxy group (—OH) for the former mechanism or the hydronium group ($—OH_3$) for the latter hop from one group site to another. The concept of proton transport by hopping is similar to the case in water via the Grotthuss mechanism and in Nafion through sulfonic acid (SO_3H) [45]. In addition, we do not rule out a mixing mechanism (i.e., epoxy-water-mediated proton transport). In the

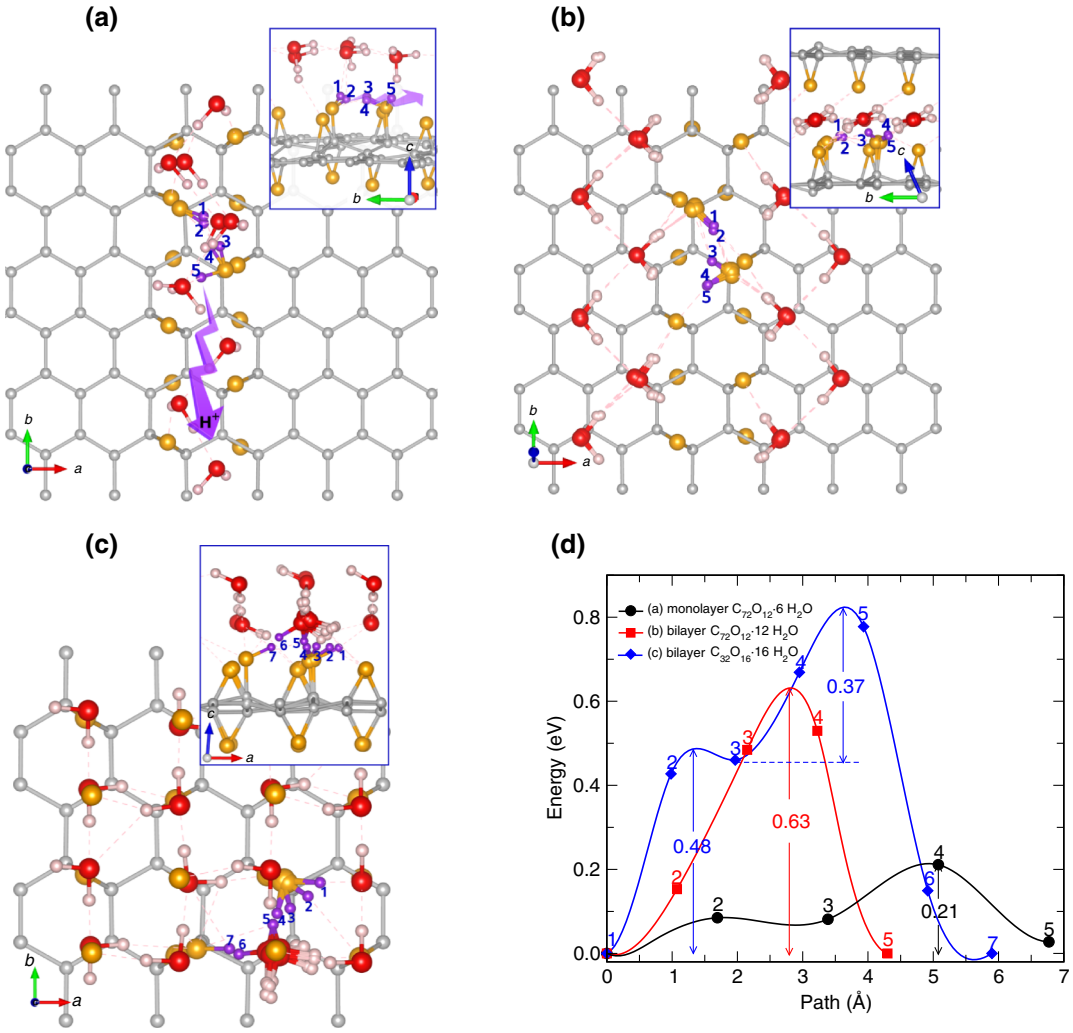

FIG. 6. Top view of migration paths for epoxy-mediated proton transport in (a) monolayer $C_{72}O_{12} \cdot 6H_2O$, (b) bilayer $C_{72}O_{12} \cdot 12H_2O$, and (c) bilayer $C_{32}O_{16} \cdot 16H_2O$ rGO sheets. The insets show the perspective view, and arrows indicate the path. (d) Activation energies for these proton migrations.

former case, we follow the same procedure as in the case of the above-mentioned anhydrous-rGO sheet, whereas in the latter case we perform ΔBVS analysis to predict the adsorption sites and migration paths of protons.

The activation barrier for epoxy-mediated proton migration in the monolayer $C_{72}O_{12} \cdot 6H_2O$ model is 0.21 eV, which is lower than that in its anhydrous counterpart, the $C_{72}O_{12}$ model (0.35 eV) (Fig. 6). Such enhancement of proton migration is attributed to hydrogen-bonding interaction between the proton and adsorbed water molecules that are placed over epoxy groups, forming a hydrogen-bonded water channel. In contrast, the activation energy in the case of the bilayer $C_{72}O_{12} \cdot 12H_2O$ model is higher, 0.63 eV. By inspecting the migration path, we find that unlike the former case there is no hydrogen bond between the proton and the intercalated water molecule in this model, in which water molecules are placed an interlayer space away from the row of epoxy groups. In the case of bilayer $C_{32}O_{16} \cdot 16H_2O$, proton migration is realized according to the epoxy-water-mediated mechanism, although we enforce epoxy-mediated migration. The activation energies are estimated to be 0.48 eV for proton movement from water to the epoxy group, which occurs without hydrogen-bonding interaction, and 0.37 eV along the epoxy-mediated path with the effect of a hydrogen bond. These results indicate that the hydrogen-bonding interaction between the proton and the water molecule can enhance in-plane proton transport.

Finally, we present the results for water-mediated proton transport in the monolayer $C_{72}O_{12} \cdot 6H_2O$ and bilayer $C_{72}O_{12} \cdot 12H_2O$ and $C_{32}O_{16} \cdot 16H_2O$ models in Figs. 7(a)–7(c). As mentioned above, water molecules are connected to their neighbors by hydrogen bonds, forming a

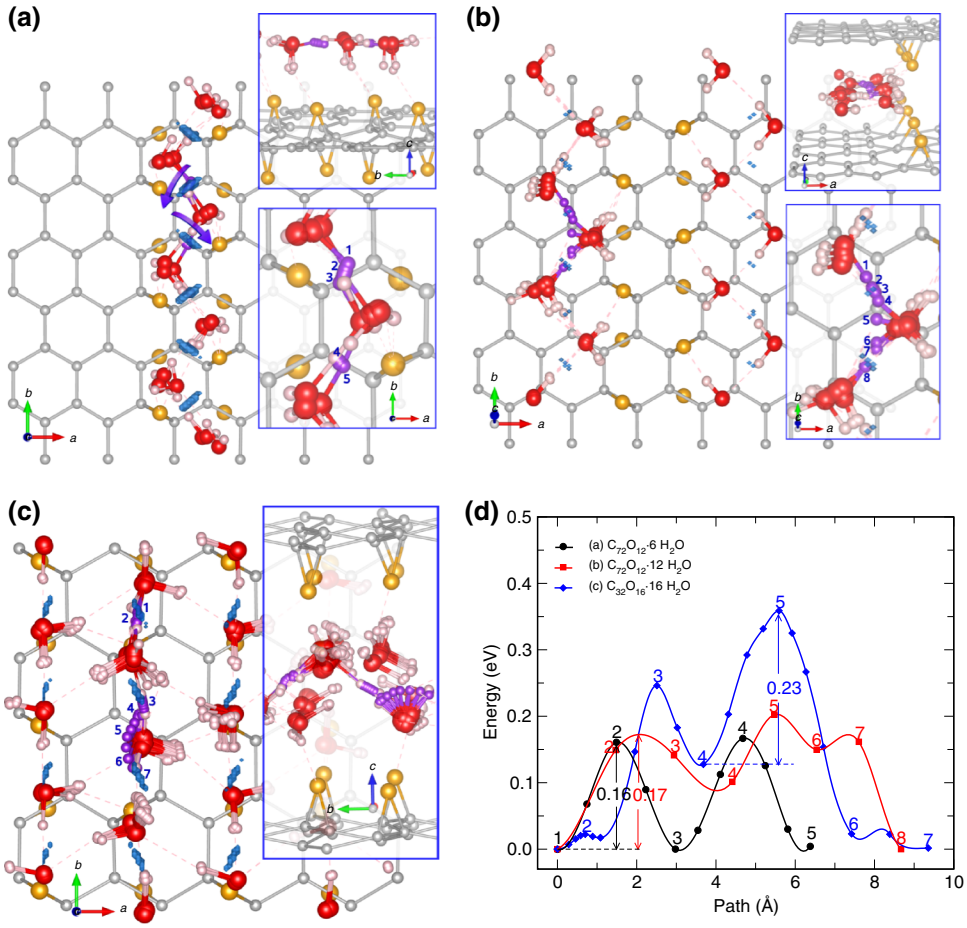

FIG. 7. Top view of migration paths for water-mediated proton transport in (a) monolayer $C_{72}O_{12} \cdot 6H_2O$, (b) bilayer $C_{72}O_{12} \cdot 12H_2O$, and (c) $C_{32}O_{16} \cdot 16H_2O$. The insets show the perspective view, and blue isosurfaces in (a),(b) represent the ΔBVS at a value of 3. (d) Activation energies for these proton migrations.

zigzag-type two-dimensional channel on top of the epoxy group in the case of monolayer $C_{72}O_{12} \cdot 6H_2O$ and bilayer $C_{32}O_{16} \cdot 16H_2O$ or in the interlayer space in the case of $C_{72}O_{12} \cdot 12H_2O$. As clarified by ΔBVS analysis, the inserted proton attaches to the water molecule with adsorption energies of −7.39, −13.11, and −12.76 eV in these sheets, forming a hydronium ion (H_3O^+), and then the nearest of its three hydrogen atoms moves to the neighboring water molecule. Rotation of water molecules to some degree is observed during the proton hopping. As shown in Fig. 7(d), the corresponding activation energies are calculated to be 0.16, 0.17, and 0.23 eV in these hydrous-rGO sheets, being much lower than along the epoxy-mediated paths and in the anhydrous-GO sheet. Moreover, they are comparable with the experimental value of 0.12 eV [26]. The similar values in monolayer $C_{72}O_{12} \cdot 6H_2O$ and bilayer $C_{72}O_{12} \cdot 12H_2O$ can be explained by the similar water-mediated paths, evidencing an indirect effect of epoxy groups, which play a role in holding the water molecules. The slightly higher value in bilayer $C_{32}O_{16} \cdot 16H_2O$ indicates that too many water molecules around the path may disturb the proton hopping due to attraction of the proton by another water molecule through hydrogen-bonding interaction.

In Table I, we summarize the main result for rGO and hydrous-rGO models with their oxidation degrees and water contents, including the interlayer distance in the bilayer models and the activation energy for the in-plane proton transport. It is revealed that the in-plane proton conductivity is enhanced through the hydrogen-bonding interaction between the proton and water when mediated by water in humid conditions. There are several options to further enhance the in-plane proton conductivity (e.g., by functionalizing GO films with sulfonic acid groups).

TABLE I. Overview of calculation data for rGO and the series of water-adsorbed rGO models with oxidation degree [O/(C + O)] and water content. The interlayer distance (d) and activation energy (E_a) are given.

Model	Layer type	O/(C + O) (%)	Water (wt%)	d (nm)	E_a (eV)
$C_{72}O_{12}$	Monolayer	14.3	...	...	0.35
$C_{72}O_{12} \cdot 6H_2O$	Monolayer	14.3	9.3	...	0.16
$C_{72}O_{12} \cdot 12H_2O$	Bilayer	14.3	17.0	0.61	0.17
$C_{32}O_8 \cdot 8H_2O$	Bilayer	20.0	21.9	0.71	...
$C_{32}O_{12} \cdot 12H_2O$	Bilayer	27.3	27.3	0.76	...
$C_{32}O_{16} \cdot 16H_2O$	Bilayer	33.3	31.0	0.86	0.23

This work may contribute to the development of efficient solid proton-exchange membranes based on GO films. It is worth noting that smaller supercells (C_{32} models) yield a slightly higher activation barrier compared with larger supercells (C_{72} models), due to an enhancement of periodic image interaction. Quantitative analysis of the influence of different concentrations of water molecules on in-plane proton conductivity should be performed.

IV. CONCLUSIONS

In conclusion, we study the atomic structures of water-adsorbed monolayer and water-intercalated bilayer rGO sheets, varying the oxidation degree and water content, and calculate the activation energies for in-plane proton transport using the first-principles method. Our calculations agree well with the experimental results for the interlayer distances of a bilayer series with increasing oxidation degree, shedding light on the hydrogen bond between the water molecule and the epoxy group. We suggest that in these hydrous-rGO sheets the proton can hop by two different mechanisms, epoxy-mediated and water-mediated paths, and conclude that water-mediated proton transport is more likely to occur due to its much lower activation energy (0.16, 0.17 eV) compared with epoxy-mediated transport, which is close to that in experiments. Our study may contribute to the understanding of the proton-conductivity enhancement of rGO films in humid conditions, and reveals new prospects for developing efficient solid proton-exchange membranes based on GO films.

ACKNOWLEDGMENTS

This work was supported as part of the fundamental research project Design of Innovative Functional Materials for Energy and Environmental Application (Grant No. 2016-20) funded by the State Committee of Science and Technology, Democratic People's Republic of Korea. Computation was done on the HP BladeSystem C7000 (HP BL460c) owned by the Faculty of Materials Science, Kim Il Sung University.

[1] K. A. Mauritz and R. B. Moore, State of understanding of Nafion, Chem. Rev. **104**, 4535 (2004).

[2] D. C. Lee, H. N. Yang, S. H. Park, and W. J. Kim, Nafion/graphene oxide composite membranes for low humidifying polymer electrolyte membrane fuel cell, J. Membr. Sci. **452**, 20 (2014).

[3] I. Nicotera, C. Simari, L. Coppola, P. Zygouri, D. Gournis, S. Brutti, F. D. Minuto, A. S. Aricó, D. Sebastian, and V. Baglio, Sulfonated graphene oxide platelets in Nafion nanocomposite membrane: Advantages for application in direct methanol fuel cells, J. Phys. Chem. C **118**, 24357 (2014).

[4] R. K. Joshi, P. Carbone, F. C. Wang, V. G. Kravets, Y. Su, I. V. Grigorieva, H. A. Wu, A. K. Geim, and R. R. Nair, Precise and ultrafast molecular sieving through graphene oxide membranes, Science **343**, 752 (2014).

[5] H. W. Kim, H. W. Yoon, S. M. Yoon, B. M. Yoo, B. K. Ahn, Y. H. Cho, H. J. Shin, H. Yang, U. Paik, S. Kwon, *et al.*, Selective gas transport through few-layered graphene and graphene oxide membranes, Science **342**, 91 (2013).

[6] H. Li, Z. N. Song, X. J. Zhang, Y. Huang, S. G. Li, Y. T. Mao, H. J. Ploehn, Y. Bao, and M. Yu, Ultrathin molecular-sieving graphene oxide membranes for selective hydrogen separation, Science **342**, 95 (2013).

[7] S. M. Holmes, P. Balakrishnan, V. Kalangi, X. Zhang, M. Lozada-Hidalgo, P. M. Ajayan, and R. R. Nair, 2D crystals significantly enhance the performance of a working fuel cell, Adv. Energy Mater. **7**, 1601216 (2017).

[8] S. Hu, M. Lozada-Hidalgo, F. C. Wang, A. Mishchenko, F. Schedin, R. R. Nair, E. W. Hill, D. W. Boukhvalov, M. I. Katsnelson, R. A. W. Dryfe, *et al.*, Proton transport through one-atom-thick crystals, Nature **516**, 227 (2014).

[9] M. I. Walker, P. Braeuninger-Weimer, R. S. Weatherup, S. Hofmann, and U. F. Keyser, Measuring the proton selectivity of graphene membranes, Appl. Phys. Lett. **107**, 213104 (2015).

[10] K. Goh, H. E. Karahan, L. Wei, T.-H. Bae, A. G. Fane, R. Wang, and Y. Chen, Carbon nanomaterials for advancing separation membranes: A strategic perspective, Carbon **109**, 694 (2016).

[11] R. R. Nair, H. A. Wu, P. N. Jayaram, I. V. Grigorieva, and A. K. Geim, Unimpeded permeation of water through helium-leak-tight graphene-based membrane, Science **335**, 442 (2012).

[12] L. Tsetseris and S. T. Pantelides, Graphene: An impermeable or selectively permeable membrane for atomic species?, Carbon **67**, 58 (2014).

[13] V. Berry, Impermeability of graphene and its applications, Carbon **62**, 1 (2013).

[14] M. Miao, M. B. Nardelli, Q. Wang, and Y. Liu, First principles study of the permeability of graphene to hydrogen atoms, Phys. Chem. Chem. Phys. **15**, 16132 (2013).

[15] W. L. Wang and E. Kaxiras, Graphene hydrate: Theoretical prediction of a new insulating form of graphene, New J. Phys. **12**, 125012 (2010).

[16] J. M. Kroes, A. Fasolino, and M. I. Katsnelson, Density functional based simulations of proton permeation of graphene and hexagonal boron nitride, Phys. Chem. Chem. Phys. **19**, 5813 (2017).

[17] L. Shi, A. Xu, G. Chen, and T. Zhao, Theoretical understanding of mechanisms of proton exchange membranes made of 2D crystals with ultrahigh selectivity, J. Phys. Chem. Lett. **8**, 4354 (2017).

[18] T. Yang, H. Lin, X. Zheng, K. P. Loh, and B. Jia, Tailoring pores in graphene-based materials: From generation to applications, J. Mater. Chem. A **5**, 16537 (2017).

[19] K. Hatakeyama, M. R. Karim, C. Ogata, H. Tateishi, A. Funatsu, T. Taniguchi, M. Koinuma, S. Hayami, and Y. Matsumoto, Proton conductivities of graphene oxide nanosheets: Single, multilayer, and modified nanosheets, Angew. Chem. Int. Ed. **53**, 6997 (2014).

[20] Y. Zhao and T. Gennett, Water-mediated Cooperative Migration of Chemisorbed Hydrogen on Graphene, Phys. Rev. Lett. **112**, 076101 (2014).
[21] Ž. Šljivančanin, A. S. Milošević, Z. S. Popović, and F. R. Vukajlović, Binding of atomic oxygen on graphene from small epoxy clusters to a fully oxidized surface, Carbon **54**, 482 (2013).
[22] L. Wang, Y. Y. Sun, K. Lee, D. West, Z. F. Chen, J. J. Zhao, and S. B. Zhang, Stability of graphene oxide phases from first-principles calculations, Phys. Rev. B **82**, 161406 (2010).
[23] M. Topsakal and S. Ciraci, Domain formation on oxidized graphene, Phys. Rev. B **86**, 205402 (2012).
[24] A. M. Dimiev, L. B. Alemany, and J. M. Tour, Graphene oxide. Origin of acidity, its instability in water, and a new dynamic structural model, ACS Nano **7**, 576 (2013).
[25] K. Raidongia and J. Huang, Nanofluidic ion transport through reconstructed layered materials, J. Am. Chem. Soc. **134**, 16528 (2012).
[26] K. Hatakeyama, M. R. Karim, C. Ogata, H. Tateishi, T. Taniguchi, M. Koinuma, S. Hayami, and Y. Matsumoto, Optimization of proton conductivity in graphene oxide by filling sulfate ions, Chem. Commun. **50**, 14527 (2014).
[27] K. Hatakeyama, H. Tateishi, T. Taniguchi, M. Koinuma, T. Kida, S. Hayami, H. Yokoi, and Y. Matsumoto, Tunable graphene oxide proton/electron mixed conductor that functions at room temperature, Chem. Mater. **26**, 5598 (2014).
[28] K. Hatakeyama, M. S. Islam, K. Michio, C. Ogata, T. Taniguchi, A. Funatsu, T. Kida, S. Hayami, and Y. Matsumoto, Super proton/electron mixed conduction in graphene oxide hybrids by intercalating sulfate ions, J. Mater. Chem. A **3**, 20892 (2015).
[29] M. R. Karim, K. Hatakeyama, T. Matsui, H. Takehira, T. Taniguchi, M. Koinuma, Y. Matsumoto, T. Akutagawa, T. Nakamura, S. Noro, *et al.*, Graphene oxide nanosheet with high proton conductivity, J. Am. Chem. Soc. **135**, 8097 (2013).
[30] K. Wakata, M. S. Islam, M. R. Karim, K. Hatakeyama, N. N. Rabin, R. Ohtani, M. Nakamura, M. Koinuma, and S. Hayami, Role of hydrophilic groups in acid intercalated graphene oxide as a superionic conductor, RSC Adv. **7**, 21901 (2017).
[31] M. Koinuma, C. Ogata, Y. Kamei, K. Hatakeyama, H. Tateishi, Y. Watanabe, T. Taniguchi, K. Gezuhara, S. Hayami, A. Funatsu, *et al.*, Photochemical engineering of graphene oxide nanosheets, J. Phys. Chem. C **116**, 19822 (2012).
[32] C.-Y. Tseng, Y.-S. Ye, M.-Y. Cheng, K.-Y. Kao, W.-C. Shen, J. Rick, J.-C. Chen, and B.-J. Hwang, Sulfonated polyimide proton exchange membranes with graphene oxide show improved proton conductivity, methanol crossover impedance, and mechanical properties, Adv. Energy Mater. **1**, 1220 (2011).
[33] L. Zhao, Y. Li, H. Zhang, W. Wu, J. Liu, and J. Wang, Constructing proton-conductive highways within an ionomer membrane by embedding sulfonated polymer brush modified graphene oxide, J. Power Sources **286**, 445 (2015).
[34] J. Klimeš, D. R. Bowler, and A. Michaelides, Van der Waals density functionals applied to solids, Phys. Rev. B **83**, 195131 (2011).
[35] I. D. Brown and D. Altermatt, Bond-valence parameters obtained from a systematic analysis of the inorganic crystal structure database, Acta Crystallogr. B. Struct. Sci. **41**, 244 (1985).
[36] G. Henkelman, B. P. Uberuaga, and H. Jónsson, A climbing image nudged elastic band method for finding saddle points and minimum energy paths, J. Chem. Phys. **113**, 9901 (2000).
[37] P. Giannozzi, S. Baroni, N. Bonini, M. Calandra, R. Car, *et al.*, QUANTUM ESPRESSO: A modular and open-source software project for quantum simulations of materials, J. Phys.: Condens. Matter **21**, 395502 (2009).
[38] We use C.pbe-van_ak.UPF, O.pbe-van_ak.UPF, and H.pbe-van_ak.UPF, which are provided in the package.
[39] J. P. Perdew, K. Burke, and M. Ernzerhof, Generalized Gradient Approximation Made Simple, Phys. Rev. Lett. **77**, 3865 (1996).
[40] M. O'Keeffe and N. E. Brese, Atom sizes and bond lengths in molecules and crystals, J. Am. Chem. Soc. **113**, 3226 (1991).
[41] G. S. Rohrer, *Structure and Bonding in Crystalline Materials* (Cambridge University Press, 2004).
[42] A. Paneri and S. Moghaddam, Impact of synthesis conditions on physicochemical and transport characteristics of graphene oxide laminates, Carbon **86**, 245 (2015).
[43] A. Paneri, Y. Heo, G. Ehlert, A. Cottrill, H. Sodano, P. Pintauro, and S. Moghaddam, Proton selective ionic graphene-based membrane for high concentration direct methanol fuel cells, J. Memb. Sci. **467**, 217 (2014).
[44] J.-A. Yan, L. Xian, and M. Y. Chou, Structural and Electronic Properties of Oxidized Graphene, Phys. Rev. Lett. **103**, 086802 (2009).
[45] S. Hu, Ph.D. thesis, School of Physics and Astronomy, The University of Manchester, 2014.